Zeeman Relaxation of CaF in Low-Temperature Collisions with Helium

Kenneth Maussang,[1,3] Dima Egorov,[1,3] Joel S. Helton,[2,3] Scott V. Nguyen,[1,3] and John M. Doyle[1,3]

[1]*Department of Physics, Harvard University, Cambridge, Massachusetts 02138, USA*
[2]*Department of Physics, MIT, Cambridge, Massachusetts 02139, USA*
[3]*Harvard-MIT Center for Ultracold Atoms, Cambridge, Massachusetts 02138, USA*
(Received 10 November 2004; published 29 March 2005)

The collision-induced Zeeman relaxation rate for collisions of CaF $X^2\Sigma(v'' = 0)$ with ^{3}He is measured to be $\Gamma_Z = (7.7 + 5.4/ - 2.5) \times 10^{-15}$ cm^3/s at 2 K. This rate is a direct measurement of the influence of spin-rotation coupling on Zeeman relaxation in the first rotational level of CaF. The relationship of this rate to known molecular constants is consistent with recent theory of cold molecular collisions and outlines the $^2\Sigma$ molecules conducive to magnetic trapping.

The production of cold polar molecules promises to impact several areas of physics and chemistry. The large electric dipole moments of polar molecules produce a strong interaction that can be exploited for quantum computing [1] or as a source for direct BCS pairing in quantum degenerate molecular matter [2–5]. Also, precision spectroscopy of heavy dipolar molecules in searches for an elementary particle electric dipole moment holds tremendous promise for observing physics beyond the standard model [6–8]. In the ultracold regime, even the smallest activation energy will exceed the available thermal energy. Tunneling becomes the dominant reaction pathway, leading to the exciting possibility of controlling chemical reactions [9,10]. Considerable progress has been made in the direct cooling of molecules, yielding larger numbers and colder temperatures in the milli-Kelvin range [11–13]. In addition, photoassociation of bialkali mixtures has produced molecules already in the ultracold regime, though vibrationally hot [14,15]. Ideally there would exist a ready source of cold molecules of any desired molecular compound that is cold and dense. To achieve this goal, a better understanding of the physics of cold molecular collisions is vital.

While a considerable amount of theoretical work has been done on cold molecular collisions, due to the technical challenges of producing samples of cold molecules, there exists scant experimental data on this subject, despite its central role in the growing field of cold polar molecules [16]. At low temperatures, the collision dynamics are sensitive to the long-range attractive part of the interaction potential, requiring a quantum mechanical treatment that takes into account all degrees of freedom and the couplings between them. Measurements of low-temperature collision rates thus provide a benchmark for quantum mechanical theories of molecular collisions. In particular, low-temperature inelastic molecular collisions are of interest because of their role in the cooling and trapping of molecules. In order to magnetically trap molecules, they must be stable against reorientation of their magnetic moments in collisions with other trapped molecules or sympathetic

atomic coolant. The reorientation of polar molecules, called Zeeman relaxation, is of critical importance as it determines the possibilities for evaporative cooling in a magnetic trap—key to the production of quantum degenerate polar matter.

Buffer-gas cooling and trapping [17] is one technique that has been shown to cool molecules and load them into a magnetic trap [18]. The cooling process relies solely on elastic collisions between molecules and cold helium gas, and so it does not require the molecules to have a particular energy level structure or atomic composition. In principle, buffer-gas trapping is applicable to any paramagnetic molecule with a Zeeman sublevel whose energy increases with increasing magnetic field. Such a level is referred to as a low-field seeking state (LFS), whereas a sublevel with decreasing energy is referred to as a high-field seeking state (HFS). However, while collisions with the buffer gas drive translational thermalization and subsequent trapping, they may also induce transitions from the low-field seeking state into the lower energy high-field seeking state. As only molecules in the low-field seeking states are trapped, collision-induced Zeeman relaxation leads to trap loss. In current implementations of buffer-gas trapping, the combined processes of translational thermalization and thermal isolation requires a ratio of elastic-to-inelastic collisions of $\sigma_{el}/\sigma_{in} \geq 10^4$ [19]. The Zeeman relaxation rate is therefore a critical parameter in deciding whether a given molecule is suitable for trapping. This rate also indicates how effective evaporative cooling will be in a trapped molecular gas.

Data on Zeeman relaxation rates in cold molecular collisions have thus far been limited to a single measurement in CaH($X^2\Sigma^+$)-He collisions at 0.4 K [18,20]. Because of the difficulty in calculating detailed molecular potentials, theoretical predictions have been made for only a limited number of molecules [21–23]. These calculations indicate that Zeeman relaxation in $^2\Sigma$ molecules occurs via the spin-rotation interaction $\gamma_{sr}\mathbf{N} \cdot \mathbf{S}$, where γ_{sr} is the spin-rotation coupling constant, $\mathbf{N}$ is the rotational angular momentum, and $\mathbf{S}$ is the electronic spin. Zeeman transi-

tions can occur directly through the excited rotational levels but vanish for the ground rotational level ($N = 0$). In Refs. [24,25], Krems *et al.* suggest that Zeeman relaxation in the ground state can still occur through ^{3}He induced electrostatic couplings between the $N = 0$ and $N = 1$ rotational levels, predicting that the Zeeman relaxation cross-section scales as γ_{sr}^2/B^4, where B is the rotational constant. In this Letter, we present a measurement of the Zeeman relaxation rate of CaF($X^2\Sigma^+$)-He collisions due to both the $N = 0$ and $N = 1$ inelastic channels, compare this measurement with molecular theory, and discuss the possibility of magnetically trapping CaF and other $^2\Sigma$ molecules.

The apparatus (shown in Fig. 1) is described in detail in Ref. [26]. CaF molecules are produced via laser ablation of calcium fluoride CaF$_2$. A cylindrical cell containing a hot-pressed powder pellet of CaF$_2$ is maintained at 0.5 K by a ^{3}He refrigerator. The cell is filled with ^{3}He gas at a typical density of 10^{16} cm^{-3}. ^{3}He density is monitored by measuring the diffusion time of laser-ablated Mn atoms through the cell [27]. An ablation beam from a pulsed frequency-doubled Nd:YAG laser with a typical pulse energy of 9 mJ is focused onto the CaF$_2$ sample. Following the ablation pulse, CaF molecules enter the helium gas, thermalize with it translationally and rotationally, and are then lost by diffusion to the cell wall with a typical $1/e$ time of $\sim$30 ms. Up to 5×10^{13}, ground-state CaF molecules are produced per ablation pulse.

The cell is placed coaxially inside the bore of a superconducting solenoid magnet which produces magnetic fields up to 4 T. The external field splits the energies of the Zeeman sublevels $X^2\Sigma^+(v = 0, N = 0, M = +1/2)$ and $X^2\Sigma^+(v = 0, N = 0, M = -1/2)$ by $\sim$1.3 K/T. Immediately following the ablation pulse, the two sublevels are equally populated since the CaF temperature during ablation is much higher than the Zeeman energy splitting. Collisions with ^{3}He atoms drive both translational thermalization and Zeeman relaxation transitions that gradually bring the populations to their equilibrium
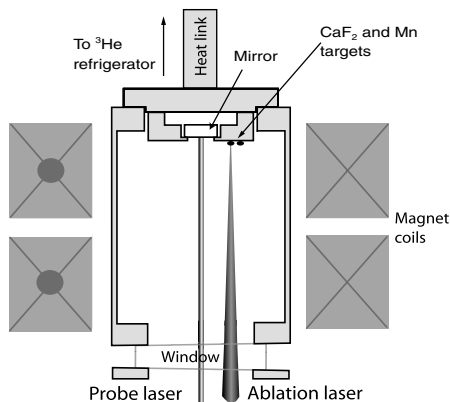
values. By observing the time dependence of the sublevel populations, we can determine the Zeeman relaxation rate.

The molecules are detected by laser absorption on the $X^2\Sigma^+(v = 0, J = 1/2, M = +1/2) \rightarrow A^2\Pi_{3/2}(v = 0, J = 3/2, M = +3/2)$ and $X^2\Sigma^+(v = 0, J = 1, M = -1/2) \rightarrow A^2\Pi_{3/2}(v = 0, N = 0, M = -3/2)$ transitions at 603 nm. A detection beam from a cavity-stabilized ring dye laser propagates along the center line of the cell. The beam is linearly polarized along the axis perpendicular to the direction of the magnetic field. Laser frequency, stabilized to the sub-MHz linewidth, is continuously scanned at a rate of 125 Hz over the absorption line. Scans are fitted to a model spectrum to extract the time dependence of the translational temperature and Zeeman sublevel populations. The relatively high accuracy of this Zeeman relaxation measurement is possible due to the fact that Zeeman shifts of the two transitions cross at 3.55 T (see Fig. 2 and Ref. [28]). With the magnetic field at 3.44 T, both transitions fall into a single scan of the laser frequency, eliminating a number of measurement uncertainties (Fig. 2).

Figure 3(a) shows the time dependence of the measured sublevel population ratio after ablation. It is convenient to define the effective spin temperature as $T_{spin} = -(\Delta E_Z/k_B)\ln[n_{LFS}/n_{HFS}]$, where n_{LFS} and n_{HFS} are populations of low- and high-field seeking states, and ΔE_Z is the energy splitting between them. The time dependence of the T_{spin} is shown in Fig. 3(b). The time dependence of the translational temperature is determined by extracting Doppler broadening from the measured spectra. As shown in Fig. 3(b), for translational temperatures near the equilibrium value, the time dependence is well described by an exponential decay $T_{tr}(t) = T_f + T_o \exp(-t/\tau_{tr})$, where T_f

FIG. 1.   Schematic of experimental apparatus. The cell is filled with $\sim$10^{16} cm^{-3} of ^{3}He buffer gas.
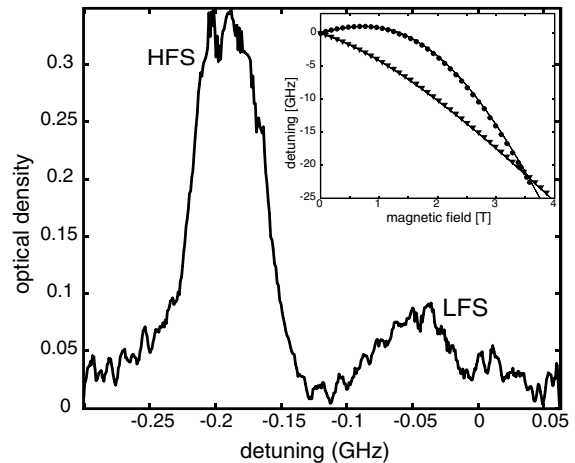

FIG. 2.   Spectrum of CaF at 3.44 T. The peak on the left is from the HFS, while the peak on the right is from the LFS. Inset: Zeeman shift of CaF. The circles mark experimental data for the LFS and triangles for the HFS, while the lines are theoretical predictions (see [28]). Zeeman relaxation measurements were performed near the crossing.
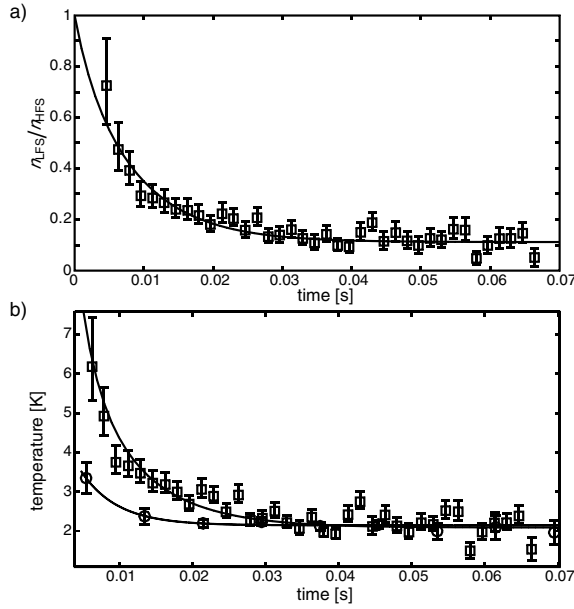
FIG. 3. (a) Dependence of the ratio of the Zeeman sublevel populations on time after ablation. The line is a fit to the rate equation solution. (b) Translational and spin temperature equilibration. The circles are translational temperatures calculated from measured Doppler broadening. The squares are spin temperatures calculated from measured Zeeman sublevel populations. The lines are fits to theoretical models.

is the equilibrium translational temperature, τ_{tr} is the thermalization time scale, and T_o is a fit parameter. Figure 3(b) shows the results of the fit; the equilibrium value of the translational temperature was measured to be $T_f = 2.0 \pm 0.3$ K. This value is higher than the steady-state cell temperature of 0.5 K. We attribute the difference to local heating by the ablation laser. This effect is observed for thermalization of laser-ablated Mn atoms as well.

In order to convert the time evolution of the relative Zeeman sublevel populations into a Zeeman relaxation rate, we adopt the following model. The ablation pulse equally populates the Zeeman sublevels. Both populations are lost on equal time scales to diffusion to the walls with a time constant τ_{diff}. In addition, low-field seekers are converted into high-field seekers due to Zeeman relaxation at a rate of Γ_Z, and vice versa due to thermal excitation at a rate of $\Gamma_Z \exp(-\Delta E_Z/k_B T_{tr})$. Because the translational temperature is comparable to the rotational spacing $[n(N = 1)/n(N = 0) \sim 0.6]$, Zeeman relaxation can occur through both the $N = 0$ channel and the $N = 1$ channel with rates $\Gamma_Z(N = 0)$ and $\Gamma_Z(N = 1)$, respectively. Zeeman relaxation through the $N = 1$ channel is a three collision process, requiring rotational excitation, Zeeman relaxation, and rotational deexcitation. However, because rotational relaxation rates in other systems are predicted to be quite large ($\sim 10^{-10}$ cm³/s) [23], we assume here that the rotational levels are always in thermal equilibrium. The three collision process for Zeeman relaxation through the

$N = 1$ channel can then be approximated as $\Gamma_Z(N = 1) \times \exp(-\Delta E_{rot}/k_B T_{tr})$, where E_{rot} is the rotational splitting. The corresponding rate equations for the two Zeeman sublevels are

$$\frac{d}{dt}(n_{LFS}) = n_{He}\left[\Gamma_Z(N = 0) + \Gamma_Z(N = 1)\exp\left(\frac{\Delta E_{rot}}{k_B T_{tr}(t)}\right)\right]$$
$$\times \left[-n_{LFS} + n_{HFS}\exp\left(\frac{\Delta E_Z}{k_B T_{tr}(t)}\right)\right] - \frac{n_{LFS}}{\tau_{diff}}, \quad (1)$$

$$\frac{d}{dt}(n_{HFS}) = n_{He}\left[\Gamma_Z(N = 0) + \Gamma_Z(N = 1)\exp\left(\frac{\Delta E_{rot}}{k_B T_{tr}(t)}\right)\right]$$
$$\times \left[n_{LFS} - n_{HFS}\exp\left(\frac{\Delta E_Z}{k_B T_{tr}(t)}\right)\right] - \frac{n_{HFS}}{\tau_{diff}}, \quad (2)$$

where n_{He} is the ³He density and $T_{tr}(t)$ is the translational temperature of the CaF molecules. We define the total Zeeman relaxation rate as the sum of the $N = 0$ rate and the $N = 1$ rate, $\Gamma_Z = \Gamma_Z(N = 0) + \Gamma_Z(N = 1) \times \exp[\Delta E_{rot}/k_B T_{tr}(t)]$. From Eqs. (1) and (2), the population ratio $R = n_{LFS}/n_{HFS}$ can easily be shown to follow

$$\frac{d}{dt}R = n_{He}\Gamma_Z[(1 + R)e^{[\Delta E_Z/k_B T_{tr}(t)]} - R - R^2] \quad (3)$$

with the initial condition $(\frac{n_{LFS}}{n_{HFS}})|_{t=0} = 1$, where $t = 0$ is the time of the ablation pulse. Equation (3) can be numerically integrated for given values of n_{He}, $T_{tr}(t)$, and Γ_Z. A least-squares fit of the measured time evolution of the population ratio with Γ_Z as the fit parameter yields a Zeeman relaxation rate of $\Gamma_Z = (7.7 + 5.4/ - 2.5) \times 10^{-15}$ cm³/s, corresponding to a cross section of $\sigma_Z^{CaF\text{-}He} = (6.3 + 4.4/ - 2.1) \times 10^{-19}$ cm². The dominant source of systematic error is our method for determining n_{He}, which relies on knowledge of the Mn-He diffusion cross section [27].

By comparing the diffusion time of CaF and Mn for a range of n_{He}, we are able to determine the diffusion cross section for CaF-He collisions to be $\sigma_{diff}^{CaF\text{-}He} = (8.1 + 5.7/ - 2.4) \times 10^{-15}$ cm². The ratio of elastic-to-inelastic collisions for CaF then is $\sigma_{diff}^{CaF\text{-}He}/\sigma_Z^{CaF\text{-}He} = (1.3 + 1.3/ - 0.5) \times 10^4$.

The measured value for $\Gamma_Z^{CaF\text{-}He}$ is much larger than the previously measured value for the Zeeman relaxation rate of CaH at 0.4 K of $\Gamma_Z^{CaH\text{-}He} = 10^{-17\pm1}$ cm³/s [20]. The molecular constants relevant to Zeeman relaxation for these two molecules are different. CaH has a large rotational splitting of $B^{CaH} = 4.277$ cm⁻¹ compared to CaF, $B^{CaF} = 0.339$ cm⁻¹ [29]. At 0.4 K the Boltzmann factor for the $N = 1$ state in CaH is $\sim 10^{-14}$. Zeeman relaxation in the CaH measurement must proceed through the $N = 0$ channel. As stated previously, at 2 K Zeeman relaxation in CaF will occur through both the $N = 0$ and $N = 1$ channels. Since the ground-state channel is a second-order process, $\Gamma_Z^{CaF\text{-}He}$ should be dominated by $\Gamma_Z(N = 1)$. We

are able to place an upper bound on the $N = 0$ rate of $\Gamma_Z(N = 0) < 7.7 \times 10^{-15}$ cm^3/s.

Our measurement does allow for comparison of Zeeman relaxation in the $N = 1$ level to the spin-rotation interaction. In the $N = 1$ level, the Zeeman relaxation cross section should scale as γ_{sr}^2 [24,25]. The spin-rotation coupling constant of CaF is $\gamma_{sr}^{CaF} = 1.3 \times 10^{-3}$ cm^{-1}, while that of CaH is $\gamma_{sr}^{CaH} = 41.5 \times 10^{-3}$. Krems *et al.* have calculated a rate of $\Gamma_Z^{CaH\text{-}He}(N = 1) = (2 \pm 5) \times 10^{-12}$ cm^3/s for CaH at 0.4 K [30]. Using γ_{sr} and adjusting for the translational temperature difference, the scaling dependence predicts that $\Gamma_Z^{CaH\text{-}He}(N = 1)$ is ~500 times faster than $\Gamma_Z^{CaF\text{-}He}(N = 1)$, falling within the error allowed by both the measurement and theory.

As expected from theory, the measured CaF elastic-to-inelastic ratio is approaching the limiting value where current buffer-gas trapping techniques can successfully trap molecules. This ratio can be improved by lowering the ^{3}He buffer-gas temperature to suppress the population in the $N = 1$ rotational level. In addition, choosing $^2\Sigma$ molecules with large rotational constants such as the hydrides would further suppress the populations. Molecules with small spin-rotation constants are another possibility. However, γ_{sr} for CaF is already relatively small. Typical values for $^2\Sigma$ molecules range from $\gamma_{sr} = 0.001$ to 1 cm^{-1}. If the excited state channel can be neglected (e.g., by cooling to 0.4 K), the γ_{sr}^2/B^4 scaling of $\Gamma_Z(N = 0)$ predicted by theory points toward molecules with large rotational constants and small spin-rotation constants. Finally, new buffer-gas techniques are being developed that have fewer in-field collisions with helium [31]. As such, molecules even with very small rotational constants could be buffer-gas cooled.

In conclusion, we have measured the inelastic relaxation rate of CaF in collisions with He and find it to be consistent with theory. This measurement, taken with the previous result for CaH, indicates that molecules with low spin-rotation and/or high rotational constants are amenable to buffer-gas loading. Similarly, we can expect that molecule-molecule collision rates for species with similar molecular constants will be favorable for evaporative cooling. For trapping of other polar molecules, those with high spin rotation and low rotational constants, these findings underline the importance of using high-field-seeking traps (e.g., FORT [32] and microwave traps [33]), where inelastic two-body collisions can be avoided altogether.

[1] D. DeMille, Phys. Rev. Lett. **88**, 067901 (2002).
[2] L. Santos *et al.*, Phys. Rev. Lett. **85**, 1791 (2000).
[3] M. Baranov *et al.*, Phys. Scr. **T102**, 74 (2002).
[4] L. D. Carr, G. V. Shlyapnikov, and Y. Castin, Phys. Rev. Lett. **92**, 150404 (2004).
[5] M. A. Baranov, Ł. Dobrek, and M. Lewenstein, Phys. Rev. Lett. **92**, 250403 (2004).
[6] E. A. Hinds, Phys. Scr. **T70**, 34 (1997).
[7] J. J. Hudson *et al.*, Phys. Rev. Lett. **89**, 023003 (2002).
[8] D. DeMille *et al.*, in *Art and Symmetry in Experimental Physics: Festschrift for Eugene D. Commins*, AIP Conf. Proc. No. 596 (AIP, New York, 2001).
[9] N. Balakrishnan and A. Dalgarno, Chem. Phys. Lett. **341**, 652 (2001).
[10] E. Bodo, F. A. Gianturco, and A. Dalgarno, J. Chem. Phys. **116**, 9222 (2002).
[11] D. Egorov *et al.*, Eur. Phys. J. D **31**, 307 (2004).
[12] T. Junglen *et al.*, Eur. Phys. J. D **31**, 365 (2004).
[13] S. Y. T. van de Meerakker *et al.*, Phys. Rev. Lett. **94**, 023004 (2005).
[14] M. W. Mancini *et al.*, Phys. Rev. Lett. **92**, 133203 (2004).
[15] A. J. Kerman *et al.*, Phys. Rev. Lett. **92**, 153001 (2004).
[16] See, for example, contributions to the 2004 ITAMP Workshop on Ultracold Polar Molecules (http://itamp.harvard.edu/polar/polar.html).
[17] R. deCarvalho *et al.*, Eur. Phys. J. D **7**, 289 (1999).
[18] J. D. Weinstein *et al.*, Nature (London) **395**, 148 (1998).
[19] C. I. Hancox *et al.*, Nature (London) **431**, 281 (2004).
[20] J. D. Weinstein, Ph.D. thesis, Harvard University, 2002.
[21] R. V. Krems *et al.*, Phys. Rev. A **68**, 051401(R) (2003).
[22] J. L. Bohn, Phys. Rev. A **62**, 032701 (2000).
[23] N. Balakrishnan *et al.*, J. Chem. Phys. **118**, 7386 (2003).
[24] R. V. Krems and A. Dalgarno, J. Chem. Phys. **120**, 2296 (2004).
[25] R. V. Krems *et al.*, Phys. Rev. A **67**, 060703(R) (2003).
[26] J. G. E. Harris *et al.*, Europhys. Lett. **67**, 198 (2004).
[27] S. V. Nguyen *et al.* (unpublished).
[28] R. V. Krems *et al.*, J. Chem. Phys. **121**, 11 639 (2004).
[29] M. Mizushima, *The Theory of Rotating Diatomic Molecules* (John Wiley & Sons, New York, 1975).
[30] R. V. Krems (unpublished).
[31] S. E. Maxwell *et al.* (unpublished).
[32] J. D. Miller, R. A. Cline, and D. J. Heinzen, Phys. Rev. A **47**, R4567 (1993).
[33] D. DeMille, D. R. Glenn, and J. Petricka, Eur. Phys. J. D **31**, 375 (2004).